Accepted for publication in Sensors and Actuators B: Chemical

Magneto-hydrodynamic Stirrer for Stationary and Moving Fluids

Shizhi Qian and Haim H. Bau*
Mechanical Engineering and Applied Mechanics
University of Pennsylvania
Philadelphia, PA 19104-6315, USA

ABSTRACT

A magneto-hydrodynamic (MHD) stirrer that exhibits chaotic advection is designed, modeled, and tested. The stirrer can operate as a stand-alone component or it can be incorporated into a MHD-controlled network. The stirrer consists of a conduit equipped with individually controlled electrodes positioned along its opposing walls. The conduit is filled with an electrolyte solution and positioned in a uniform magnetic field. When a potential difference is applied across pairs or groups of electrodes, the resulting current interacts with the magnetic field to induce Lorentz forces and fluid motion. When the potential difference is applied across opposing electrodes that face each other, the fluid is propelled along the conduit's length. When the potential difference is applied across diagonally positioned electrodes, a circulatory motion results. When the potential difference alternates periodically across two or more such configurations, chaotic motion evolves and efficient mixing is obtained. This device can serve as both a stirrer and a pump. The advantage of this device over previous designs of MHD stirrers is that it does not require electrodes positioned away from the conduit's walls. Since this device has no moving parts, the concept is especially suitable for microfluidic applications.

Keywords: Microfluidics, magneto-hydrodynamics (MHD), chaotic stirrer, microreactors, lab on a chip

* Corresponding author. E-mail address: bau@seas.upenn.edu

1. INTRODUCTION

In recent years, there has been a growing interest in microfluidic systems (laboratories on chips) for bio-detection, biotechnology, chemical reactors, and medical, pharmaceutical, and environmental monitors. In many of these applications, it is necessary to propel fluids and particles from one part of the device to another, control the fluid motion, stir, and separate fluids. In microdevices, these tasks are far from trivial. Magneto-hydrodynamics (MHD) offers a convenient means of performing some of these functions.

The application of electromagnetic forces to pump, confine, and control fluids is by no means new. MHD is, however, mostly thought of in the context of highly conducting fluids such as liquid metals and ionized gases [1-2]. Recently, a number of researchers have constructed MHD micro-pumps on silicon and ceramic substrates and demonstrated that these pumps are able to move liquids around in small conduits [3-6]. Bau et al. [7-9] demonstrated the feasibility of using magneto-hydrodynamic (MHD) forces to control fluid flow in microfluidic networks. By judicious application of different potential differences to different electrode pairs, one can direct the liquid to flow along any desired path without a need for valves and pumps. Moreover, by circulating the fluid in a closed loop equipped with heaters that maintain different, fixed temperatures, one can produce the conditions necessary for continuous polymerase chain reaction (PCR) [5, 10].

In many applications, it is necessary to facilitate interactions among various reagents. Often diffusion alone is far too slow to achieve this task. Since the Reynolds numbers of flows in microdevices are usually very small, one is deprived of the benefits of turbulence for mixing enhancement. Gleeson and West [11] constructed and tested a torioidal MHD stirrer in which the direction of the flow reversed periodically. Such a stirrer takes advantage of Taylor dispersion [12] to increase the surface area between two interacting fluids. Alternatively, one can

pattern electrodes of various shapes that induce electric fields in different directions. The interaction of such electric fields with the magnetic field induces secondary flows that may benefit stirring and mixing [7]. Although these secondary flows significantly enhance the mixing process, they are well-ordered and the mixing is poor. One can do better, however. By periodically or aperiodically alternating among two or more different flow patterns, one can induce (Lagrangian) chaotic advection. Aref [13] described the general ideas associated with chaotic mixing, and our group implemented similar ideas in the context of microfluidic systems and MHD stirrers [14-17]. All the MHD stirrers described above require some of the electrodes to be patterned inside the conduit or cavity and away from the conduit/cavity walls. In some cases, such internal electrodes may be intrusive. To alleviate this potential shortcoming, we describe in this paper a new stirrer design that does not require any interior electrodes. The same electrodes that are used for pumping are also used for stirring. This arrangement requires fewer fabrication steps than were needed in the previous designs and it minimizes the intrusion that may be posed by internal electrodes. The newly designed MHD stirrer can operate with both stationary and with moving fluids.

The paper is organized as follows. We first simulate theoretically the flow field and study the performance of the stirrer by tracking the spatial and temporal evolution of the concentration of a reagent. Then, we describe the construction of a simple experimental apparatus. Subsequently, the theoretical predictions are compared with experimental observations.

2. THEORY

In this section, we describe a three-dimensional model of the MHD stirrer. Consider a rectangular conduit of width $2h$ and height H. See **Fig. 1** for a schematic depiction of the conduit's top view. The x, y, and z coordinates are aligned, respectively, with the conduit's axis,

width, and height. Several individually controlled electrodes denoted C_i^+ and C_i^- ($i=0, \pm1, \pm2, \ldots$) are positioned, respectively, at $y=h$ and $y=-h$ (along the conduit's opposing walls). The length of each electrode is L_E. There is a small dielectric gap of length c between adjacent electrodes. The top (C_i^+) and the bottom (C_i^-) electrodes are staggered with displacement S ($0 \le S \le L_E/2$). When $S=0$, the electrodes C_i^+ and C_i^- face each other. When $S>0$, electrodes C_i^+ and C_i^- are located diagonally from each other. The conduit is filled with at least weakly conducting electrolyte solution of electrical conductivity (σ) and viscosity (μ). The device is placed in a uniform, static magnetic field of flux density $\mathbf{B} = B\hat{e}_z$ directed in the (z) direction that is perpendicular to the x-y plane. $\hat{e}_z$ is a unit vector in the z-direction. Alternatively, instead of DC fields, one could use synchronized AC electric and magnetic fields. AC fields have the advantage of minimizing the migration of charged particles in the electric field, bubble generation, and electrode corrosion. We use bold letters to denote vectors. When current of density $\boldsymbol{J}$ (A/m^2) is transmitted through the solution, the interaction between the current and the magnetic field results in a Lorentz force of density $\boldsymbol{J}\times\boldsymbol{B}$.

When the device serves as a pump, the electrodes C_i^+ ($i= 0, \pm1, \pm2, \ldots$) are wired to form a single electrode C^+ that is connected to one terminal of a power supply. The electrodes C_i^- ($i=0, \pm1, \pm2, \ldots$) are similarly wired to form a single electrode C^-. When a potential difference ΔV is imposed between the two grouped electrodes C^+ and C^-, the current direction is nearly normal to the surface of the electrodes, the Lorentz force is directed along the conduit's axis, and the device operates as a pump. Since the Lorentz force is a body force, the resulting velocity profile has the same shape as in pressure-driven flow [6].

When only two of the electrodes are activated, say C_0^+ and C_0^-, and $L_E>S>0$, the direction of the current flow is oblique to the electrodes' surfaces and the resulting Lorentz force has a component transverse to the conduit's axis. As a result, one observes cellular flow. We will

exploit this secondary flow to enhance mixing. When $S=0$, a similar secondary flow can be obtained by activating diagonally positioned electrodes such as electrodes C_0^- and C_1^+ in Fig.1.

According to Ohm's law for a moving conductor of conductivity σ in a magnetic field, the potential difference ($\Delta V=V_1-V_2$) induces a current of density:

$$\mathbf{J} = \sigma\left(-\nabla V + \mathbf{u}\times\mathbf{B}\right). \tag{1}$$

In the above, **u** is the fluid's velocity. For incompressible flow, the continuity and momentum (Navier-Stokes) equations are, respectively,

$$\nabla \bullet \mathbf{u} = 0\,, \tag{2}$$

and

$$\rho\frac{D\mathbf{u}}{Dt} = \mathbf{J}\times\mathbf{B} - \nabla p + \mu\nabla^2\mathbf{u}\,. \tag{3}$$

In the above, t is time, p is the pressure, and ρ is the liquid's density. We specify non-slip velocity at all solid boundaries. At the conduit's walls,

$$\boldsymbol{u}(x, \pm h, z) = \boldsymbol{u}(x, y, 0) = \boldsymbol{u}(x, y, H) = 0. \tag{4}$$

We assume that the conduit's length L is large compared to its width ($L>>h$) and to the size of individual electrodes ($L>>L_E$).

We will consider two different operating conditions. In the first case, there is no net flow through the stirrer:

$$\boldsymbol{u}(\pm L/2, y, z)=0. \tag{5}$$

The zero net flow condition is applicable when there is no external driving force and the conduit is long or when one or both ends of the conduit are closed (i.e., with valves). In the second case, we will consider the presence of externally induced net flow through the device. Such flow can be driven, for example, by pressure gradients. In this circumstance, we will specify a uniform inlet velocity and a reference pressure at the exit.

$$\boldsymbol{u}(-L/2, y, z) = U\hat{e}_x . \tag{6}$$

The electric potential (V) satisfies the Laplace equation:

$$\nabla^2 V = 0. \tag{7}$$

We use insulating boundary conditions at all dielectric surfaces and specify the potentials of the active electrodes. The inactive electrodes' potentials are uniform but unknown apriori and must be determined as part of the solution process. Since the inactive electrodes cannot accumulate charge, we have on each inactive electrode the condition of zero net current flow:

$$\oint_s \nabla V \bullet \hat{n} ds = 0 . \tag{8}$$

One can take advantage of the linearity of equation (7) and use superposition to determine the unknown potentials of the inactive electrodes. We illustrate this procedure with an example. Suppose that only one electrode pair C_0^- - C_1^+ is active, $S=0$, and potentials φ_0^- and φ_1^+ are imposed, respectively, on electrodes C_0^- and C_1^+. The unknown potentials of the inactive electrodes C_i^- $(i=\pm1, \pm2,...)$ and C_i^+ $(i=0, -1, \pm2,...)$ are denoted, respectively, φ_i^- $(i=\pm1, \pm2,...)$ and φ_i^+ $(i=0,-1, \pm2,...)$, where $\varphi_i^\pm$ are constants that need to be determined. We decompose the potential into the sum:

$$V = V_1 + \sum_j \varphi_j^+ V_j^+ + \sum_j \varphi_j^- V_j^- \tag{9}$$

Each of the subproblems satisfies the Laplace equation:

$$\nabla^2 V_i^\pm = 0 . \tag{10}$$

We first solve the problem for V_1 with the boundary conditions:

$$V_1 = \begin{cases} \varphi_0^- & \text{on electrode } C_0^- \\ \varphi_1^+ & \text{on electrode } C_1^+ \\ 0 & \text{on all other electrode surfaces } C_i^\pm \end{cases} \tag{11}$$

Subsequently, we solve the Laplace equations for V_j^+ *(j =0, -1, ±2,...)* and V_j^- *(j =±1, ±2,...)* with the boundary conditions:

$$V_i^{\pm} = \begin{cases} 1 & \text{on electrode } C_i^{\pm} \\ 0 & \text{on all other electrode surfaces } C_{j\neq i}^{\pm} \end{cases} \tag{12}$$

The unknowns φ_j^- *(j=±1, ±2,...)* and φ_j^+ *(j=0, -1, ±2,...)* are then obtained from the zero net current flow conditions:

$$\oint_{s_j} \nabla V \bullet \hat{n} ds_j = 0. \tag{13}$$

Alternatively, one can solve for the potential field by implementing equations (13) directly in the finite element code. This procedure increases the number of variables in the problem to include the unspecified potentials as unknowns while using equations (13) as additional equations. When there are many electrodes with unspecified potentials, the augmented system proved to be more convenient to use. We carried out the calculations of the potential field with FEMLAB[+]. **Fig. 2** depicts contours of constant potential lines at the conduit's mid-plane (*z=H/2*) when $c/L_E=0.05$, $L/L_E=8.5$, $H/L_E=0.4$, $h/L_E=0.4$, $S=0$, $\varphi_0^-/\varphi_{\max}=1$, and $\varphi_1^+/\varphi_{\max}=0$.

Once the potential field was determined, we solved equation (1) for the current density by dropping the second term since it is much smaller than the first one and then solving equations (2) and (3) for the velocity field.

Trajectories of passive tracer particles are then obtained by integrating the kinematic equations,

$$\frac{d\mathbf{x}}{dt} = \mathbf{u}(\mathbf{x}, t), \tag{14}$$

[+] FEMLAB is a product of Comsol Inc., Sweden

where **x**={x,y,z} is the position vector.

Fig. 3 depicts trajectories of passive tracer particles injected into the fluid at various locations at the conduit's mid-height ($z=\frac{H}{2}$) in the absence of through flow. The conditions are the same as in Fig. 2. The flow field was computed with the computational fluid dynamics software CFD-ACE*. Clearly, the MHD flow is effective in moving material from one side of the conduit to the other. For example, when half of the conduit is initially filled with species *M* and the other half with species *N*, the interface stretches and deforms to form spiral like tongues with one material penetrating into the other similar to the pattern depicted in Fig. 10 of [7]. We refer to the flow pattern depicted in Fig. 3 as flow pattern **A** and to the corresponding velocity field as $\mathbf{u}_A$. A nearly mirror image of the flow pattern depicted in Fig. 3 forms when one applies the potential difference across the diagonal electrodes C_{-1}^{+} and C_0^{-}. We refer to the latter flow pattern as pattern **B** and the corresponding velocity field as $\mathbf{u}_B$.

When either flow pattern **A** or **B** acts alone, it does, indeed, advect material from one side of the conduit to the other, enhancing mixing. Although much faster than diffusion alone, the stretching rate of the interface between the two fluids *M* and *N* is still relatively slow and scales approximately like *(t+1)ln(t+1)* [7]. One can do better, however. By periodically or aperiodically alternating between flow patterns **A** and **B**, one can obtain more complicated trajectories of the passive tracer particles and achieve chaotic advection which elongates the length of the interface between *M* and *N* at an exponential rate.

Here, we use the temporally periodic protocol:

$$\left.\begin{aligned} \varphi_0^- = \Delta V, \text{ and } \varphi_1^+ = 0, \quad (\mathrm{kT} < \mathrm{t} < \mathrm{kT} + \frac{\mathrm{T}}{2}) \\ \varphi_{-1}^+ = \Delta V, \text{ and } \varphi_0^- = 0. \quad (\mathrm{kT} + \frac{\mathrm{T}}{2} < \mathrm{t} < (\mathrm{k}+1)\mathrm{T}) \end{aligned}\right\}, \tag{15}$$

* CFD-ACE is a product of CFDRC Inc. USA

where k is an integer ($k=0,1,...$), and T is the period. During the first half period, electrode $C\text{-}_1^+$ is disconnected, and the electrode pair C_0^- and C_1^+ is active with a potential difference ΔV_1. In the second half period, electrode C_1^+ is disconnected, and the electrode pair $C\text{-}_1^+$ and C_0^- is active with a potential difference ΔV_2. We will study only the special case of $\Delta V_1=\Delta V_2=\Delta V$. The protocol described by equation (15) is just one example of numerous possibilities. The choice of the most effective protocol is an interesting optimization problem that we do not address here.

To visualize the stirrer's action, we follow the rate of spread of a reagent in the stirring zone. We denote the dimensionless concentration of the species with G. The concentration is normalized with its largest value. Let the dark color (Fig. 4) denote the absence of species G (G(**x**, t)=0) and the light color indicate the presence of species G at its highest concentration ($G(\mathbf{x},t)=1$). Initially (Fig. 4a), the dark color fluid occupies the conduit's lower section ($y<0$) and the light color fluid occupies the conduit's upper section ($y>0$).

$$G(x,y,z,0)=\begin{cases}0, & y<0\\ 1, & y>0\end{cases}. \tag{16}$$

To track the stirring process, we solve the advection equation

$$\frac{\partial G}{\partial t}+\mathbf{u}\cdot\nabla G=D\nabla^2 G, \tag{17}$$

with the boundary conditions $\nabla G\bullet\hat{n}=0$ at all solid boundaries and $\left(-D\nabla G+\mathbf{u}G\right)\bullet\hat{n}=0$ at $x=\pm L/2$, where, typically, $L/L_E\sim 8$. In the above, D is the molecular diffusion coefficient, and we assume that the fluid's properties are not significantly affected by the change in the concentration of the dissolved species.

Fig. 4 depicts the concentration $G(x,y,H/2,t)$ as a function of x and y at times $t=0$ (a), $T/4$ (b), $T/2$ (c), $3T/4$ (d), and T (e) when the two pairs of electrodes $C_0^-\text{-}C_1^+$ and $C\text{-}_1^+\text{-}C_0^-$ are actuated alternately with a period $T=4s$ and there is no net flow. The diffusion coefficient $D=1.0\times10^{-11}m^2/s$; the imposed potential difference $\Delta V=2.5V$; the length of an individual electrode is

L_E=*10mm*; the gap between adjacent electrodes *c=0.5mm*; the displacement *S=0*; and the length, width, and height of the conduit are, respectively, *L=85mm*, *2h*=8*mm*, and *H=4mm*. The figure illustrates rapid mixing in the stirred region. Within one period, the distinction between the dark and light has nearly disappeared in the stirring region. Away from the stirring region, the two fluids remain well separated. The engagement of a larger number of electrodes would increase the volume of the stirred fluid.

Fig. 5 depicts the evolution of the concentration distribution at various cross-sections that are perpendicular to the conduit's axis and located at $x=1.5L_E+c$ (top row), *x=0* (center row), and $x=-(1.5L_E+c)$ (bottom row). Columns a, b, c, d, and e, correspond, respectively to times *t=0, T/4, T/2, 3T/4,* and *T*. The cross-sections located at $x=1.5L_E+c$ (top row) and $x= -(1.5L_E+c)$ (bottom row) do not exhibit identical behavior because the cross-section at $x=1.5L_E+c$ is closer to the electrodes that are activated during the first half of the period. Thus, the interface between the two fluids in the upper row deforms as soon as the first pair of electrodes is engaged. The cross-section at $x=-(1.5L_E+c)$ starts to see action only during the second half of the period. The figure illustrates that the stirring phenomenon is three-dimensional.

To quantify the stirrer's performance, we define the mixing quality α [18]:

$$\alpha(x,t) = 1 - \frac{st(x,t)}{st(x,0)} \tag{18}$$

where $st^2(x,t)$ is the standard deviation of the dimensionless concentration distribution at time *t* and at a cross- section located at *x*. $st^2(x,t) = \int_0^H \int_{-h}^{h} \left(G(x,y,z,t) - \overline{G}(x,t)\right)^2 dydz$, and $\overline{G}(x,t)$ is the *y-z* average cross-sectional concentration. The maximum value of $st^2(x,t)$ occurs when *t=0*. When *t=0,* $\alpha=0$. When the species are well mixed, $st(x,t) = 0$ and $\alpha=1$. Thus, $0 \le \alpha(x,t) \le 1$.

Fig. 6 depicts the mixing quality $\alpha(x,t)$ as a function of time when $x=\pm(1.5L_E+c)$ and *x=0*. Initially ($0<t\le T/2$), $\alpha(1.5L_E+c,t)$ (solid line) increases rapidly during the first half period

since it is closer to the electrodes C_0^--C_1^+ engaged during this time interval. In the second half period, the growth rate of $\alpha(1.5L_E+c, t)$ decreases, and then increases again in the third half period. Similar behavior is repeated by $\alpha(-1.5L_E-c, t)$ with a delay of T/2. The very low rate of increase of $\alpha(-1.5L_E-c, t)$ during the first half period ($0<t<2s$) indicates that diffusion alone plays a minor role in the stirring process. The cross-section located at $x=0$ is nearly equally affected by both flow patterns **A** and **B**. Therefore, the mixing quality at $x=0$ (dash-dot line) increases most rapidly and lacks the plateaus that are visible in the other two curves.

So far, we have described the operation of the stirrer when the only fluid motion in the conduit was due to the agitation induced by the stirrer. In other words, no through flow was present. In certain circumstances, it may be desirable to stir the fluids while it is pumped through the conduit. Such net fluid motion can either be driven by an external pressure, i.e., the fluid is pumped continuously with a syringe pump, or by a MHD drive located some distance away from the stirring region. Other researchers have achieved chaotic advection of fluids moving in micro channels by perturbing the main flow stream with time-periodic pressure perturbations [19] or exploiting electro-kinetic instabilities under high-voltage AC electric fields [20]. Here, we perturb the main stream with MHD.

We consider the case of zero electrode displacement ($S=0$). We connect all the upper, odd-numbered electrodes C_i^+ ($i=\pm1, \pm3,\ldots$) to form the single electrode "**TO**;" all the lower, odd-numbered electrodes C_i^- ($i=\pm1, \pm3,\ldots$) to form the single electrode "**BO**;" all the upper, even numbered electrodes C_i^+ ($i=0, \pm2, \pm4,\ldots$) to form the single electrode "**TE**;" and all the lower, even numbered electrodes C_i^- ($i=0, \pm2, \pm4,\ldots$) to form the single electrode "**BE**." When electrode "**TO**" is connected to one terminal of a power supply and electrode "**BE**" is connected to another terminal of the power supply, the resulting Lorentz forces have both axial and transverse components, thereby inducing both axial motion and cellular convection. **Fig. 7**

depicts the resulting flow field at the conduit's midplane ($z=H/2$) when $L=80mm$, $H=2mm$, $h=2mm$, $L_E=5mm$, $c=0.5mm$, and $S=0mm$. Eleven electrodes are patterned along the top ($y=h$) and bottom walls ($y=-h$). The pressure-driven flow is introduced with a uniform axial velocity $u(-\frac{L}{2}, y, z, t) = 5mm/s$. The distance between the entrance and the leading edge of the first electrode is $10mm$. The external magnetic field $B=0.4T$. The imposed potential differences between the electrodes **TO** and **BE** and between the electrodes **BO** and **TE** are $\Delta V=2.5V$. The conductivity of the electrolyte is $\sigma=2.56\ \Omega^{-1}m^{-1}$, and the diffusion coefficient $D=10^{-11}m^2/s$. The arrows and the solid lines depict, respectively, the velocity field and the trajectories of passive tracer particles. In the absence of temporal alternation of the electrodes' potentials, Fig. 7 illustrates that as the passive tracer particles advect downstream, they trace an oscillatory path with very little cross-stream transport. To obtain more complicated motions, we will alternately activate the electrode pairs TO-BE and BO-TE.

To quantify the stirring process, we supply into the conduit a solution such that

$$G(-\frac{L}{2}, y, z, t) = \begin{cases} 1, & y < 0 \\ 0, & y > 0 \end{cases} \tag{19}$$

with the initial condition

$$G(x, y, z, 0) = \begin{cases} 1, & y < 0 \\ 0, & y > 0 \end{cases}. \tag{20}$$

Fig. 8 depicts the concentration $G(x, y, \frac{H}{2}, t)$ at the conduit's midheight at various times t=0 (a), T/2 (b), T (c), 3T/2 (d), and 2T (e) when the electrode potentials are alternated with period T. The simulation conditions are similar to the ones detailed in Fig. 7. Fig. 8a depicts the situation before the stirring electrodes have been activated. Witness that diffusion plays a minimal role in the mixing process. The concentration distribution along the length of the conduit remains similar to the inlet distribution. Once the electrodes have been engaged ($t>0$),

the situation changes rapidly. Figures 8b, c, d, and e illustrate the rapid blending. **Fig. 9** depicts the evolution of the cross-sectional (*y-z* plane) concentration field at *x=40mm* (first row) and *x=70mm* (the second row) as functions of time *t=0, T/2, T, 3T/2,* and *2T*. Witness that most of the cross-sectional area assumes a nearly uniform color, indicating that the two species are reasonably well-mixed.

Fig. 10 depicts the mixing quality α as a function of time at the cross-sectional planes *x=10mm* (solid line and symbols ■), *x=40mm* (dashed line and symbols ●), and *x=70mm* (dash-dotted line and symbols ▲). The stirrer is activated at *t=0*. Prior to the stirrer's activation, the species were well separated (Fig. 8a) and $\alpha(0)=0$. As time increases, α initially increases rapidly until it attains an asymptotic value. The cross section *x=10mm* is at the front edge of the leading electrode (the entrance of the mixing region). At this location, little time is available for the stirring process to have an effect, and α is relatively small. To enable visibility, the curve at *x=10mm* was magnified, and the corresponding α scale is given on the RHS vertical axis of the graph. The magnitudes of α at *x=40mm* and *70mm* are much larger, and the corresponding α values are given on the LHS of the graph. The graphs in Fig. 10 provide the designer with guidance about how long the stirrer should be to achieve a desired α value.

The effectiveness of the MHD stirrer depends on the relative magnitudes of the net through flow and the secondary MHD flow. We define the ratio between the force associated with the MHD-induced secondary flow per unit length ($JBcos\theta D_H^2$) and the viscous force associated with the through flow per unit length:

$$K = \frac{JBD_H^2 \cos\theta}{\mu U}. \tag{21}$$

In the above, θ is the angle between the diagonal line that connects the centers of the active pair's electrodes and the y-axis, J is the current density, B is the intensity of the magnetic field, *U*

is the inlet, average axial velocity, μ is the liquid's viscosity, and D_H is the hydraulic diameter of the conduit.

Fig. 11 depicts the mixing quality α at $x=40mm$ and t=$16s$ as a function of K. When K is small ($K<<1$), through flow effects dominate, the MHD secondary flow has little effect, and α remains small. When 0.8>K>0.2, α increases nearly linearly as K increases. When K>2, α achieves an asymptotic value. The figure indicates that to achieve effective stirring, K must be larger than 1.

In the above examples, only two groups of electrodes were activated. More complicated flow topologies will form when more than two groups are engaged. The selection of the various parameters such as the gap distance (c) between adjacent electrodes, the displacement (S), the electrode length (L_E), the number of electrode pairs, the stirring protocol, and the dimensions of the conduit that provide the most efficient stirring process is an interesting optimization problem that we do not address here.

α is only one figure of merit for the stirrer's performance. Another important consideration is the energy consumption of the stirrer. In the case of the MHD stirrer, the energy consumption depends on the choice of the electrolyte and electrode materials. In fact, with appropriate choice of electrodes and electrolytes, the stirrer can form a galvanic cell, be self-driven, and actually produce electrical energy while performing the stirring (or pumping) function. A few examples of possible choices of electrodes and electrolytes that would lead to electric energy production are stainless steel and zinc electrodes operating with a strong oxidizer such as $Fe(NO_3)_3$ or an acid as an electrolyte.

3. EXPERIMENTAL SET-UP

To illustrate that similar flows to the ones predicted in the previous section can be observed in practice, we fabricated two prototypes of MHD stirrers with elastomer Polydimethylsiloxane (PDMS, Dow Corning Sylgard Elastomer 184, base and a curing agent with volume ratio 10:1). PDMS has been widely used to form microfluidic components, and it provides a convenient platform for rapid prototyping [21]. To facilitate easy flow visualization, the device was made relatively large. **Fig.12** depicts schematically the experimental device, which consists of a Y-shaped micro channel equipped with several electrodes positioned along the opposing walls.

A copper sheet was glued on a 1.5mm thick, polycarbonate slab. The copper was then machined with a computer-controlled milling machine (Fadal 88 HS) to form individual electrodes (with a gap $c=0.5mm$ between two adjacent electrodes) and electrode leads. Electrodes with lengths of 10mm and 5mm were machined. The former were used in the closed cavity experiments, and the latter in the flow through experiments.

A polycarbonate template in the shape of the stirrer cavity was milled and positioned on a glass substrate. The closed stirrer's template consisted of a rectangular slab ($L\times W\times H=85mm\times 8mm\times 2mm$) while the flow-through stirrer's template was shaped like a Y ($L\times W\times H=85mm\times 4mm\times 2mm$). The leading edge of the first electrode was $10mm$ downstream from the straight conduit's entrance (the point where the two legs of the Y connect with the third). Two plastic tubes (1.75mm O.D. and 1.2mm I.D.) were connected to the two legs of the Y. A third tube was connected to the chamber's exit. Finally, a PDMS solution was cast around the template. After curing the PDMS, the template and frame were removed, leaving behind a cavity with patterned electrodes along its sidewalls. The cavity was capped with a glass slide.

The electrodes were connected via computer-controlled relay actuators and a D/I card (PCL-725, Advantech Co., Ltd.) to the terminals of two DC-power supplies (Hewlett Packard,

HP 6032A). The relays were wired and programmed to switch "on" and "off" each group of electrodes. The device was positioned on top of a neodymium (NdFeB, Polymag Inc.), permanent magnet that provided a nearly uniform intensity magnetic field of B~0.4T. The magnetic field was measured with the aid of a gauss meter. The conduit was filled with 0.5M $CuSO_4$ electrolyte solution with a conductivity $\sigma \approx 2.56 \Omega^{-1} m^{-1}$ [22].

In the absence of through flow, the flow field was visualized by introducing either a single drop of dye or drops of dye with different colors at various locations in the conduit. In the presence of through flow, one stream with clear fluid and another stream with dye were introduced in the two legs of the Y. The flow visualization allowed us to obtain only a qualitative description of the stirring process. The images of the flow field were captured with both video and still cameras. The movies provided a much more vivid account of the evolution of the dye tracers.

4. EXPERIMENTAL OBSERVATIONS

First, we compare the predicted potential field with the potential field that actually existed in our experiments. To this end, we predicted and measured the potential of one of the inactive electrodes. **Fig.13** depicts the potential difference between the inactivate electrode C_{-1}^{+} and the ground electrode C_1^{+} as a function of the imposed potential difference ΔV between the engaged electrodes C_0^{-} and C_1^{+}. The solid line and the symbols ($\bullet$) represent, respectively, the theoretically calculated values and experimental measurements. Witness the good agreement between experiment and theory.

In the absence of through flow, **Fig. 14** depicts the flow visualization observations when electrode pairs C_0^{-}-C_1^{+} and C_{-1}^{+}-C_0^{-} were alternately actuated with a period T=4s and potential difference ΔV=2.5V. Initially, a drop of red dye was introduced into the conduit to

approximately occupy the region adjacent to a single electrode pair (*t=0*). As time increased, so did the area occupied by the dye. The figure depicts the images of the dye spread at times *t=0, T/2, T, 3T/2, 2T, 5T/2,* and *3T*. The figure illustrates the rapid stirring processes. The images are consistent with chaotic stirring. When *t=3T=12s*, the dye has occupied the entire stirring region (length of 3 electrodes). Throughout the experiment, we monitored carefully for bubble formation. No bubble production was observed.

The spread of the dye is facilitated by both diffusion and advection. To verify that diffusion alone did not play a significant role in our experiments, we introduced a drop of dye into the conduit and followed its spread without activating the stirrer. During the time interval of a typical experiment (about 40s), only a very small spread of the dye was observed. Diffusion did not appear to play a significant role in our experiments.

The stirring process is described more vividly in **Fig. 15**. Red and green dye blobs were introduced into the conduit, and their evolution was tracked as a function of time. At *t=0*, the red and the green dyes were well separated (Fig.15, t=0). After one period, some of the red dye was surrounded by the green dye (Fig. 15, t=T). As time increased, through continuous stretching and folding which are characteristic of chaotic advection, the two dyes blended.

For continuous, through-flow mixing, the two inlet legs of the Y-shaped conduit were connected to two computer-controlled syringe pumps (KDScientific Inc., model 200 series). We first filled the channel with DI water and then injected dye through one leg of the Y and clear electrolyte solution through the other leg. The total inlet flow rate was 2ml/s. When the mixer was not activated, the two streams were separate. One side of the conduit ($y<0$) was occupied with the dye while the other side ($y>0$) was occupied with the colorless electrolyte (Fig. 16a). The two fluids flowed downstream side by side with very little mixing. When the mixer was activated by alternating the electrode pairs TO-BE and BO-TE, the Lorenz force drove secondary flows, and the two streams mixed rapidly. Figs. 16b, c, and d depict the spread of the dye at

times t=T/2, T and 3T/2 when T=4s. The experimental observations (Fig.16) are in qualitative agreement with the theoretical predictions (Fig. 8).

5. DISCUSSION AND CONCLUSIONS

The paper describes a magneto-hydrodynamic stirrer that does not require any interior electrodes. The stirrer consists of a conduit filled with an electrolyte solution and positioned in a magnetic field. Individually controlled electrodes are positioned along the conduit's opposing sidewalls. By appropriate adjustment of the potential differences across the wall-electrodes, one can use the resulting Lorentz forces to either pump or stir the fluid. When a potential difference is applied across opposing electrodes, the device operates as a pump. When the potential difference is applied across two or more diagonally positioned electrodes, secondary flows are induced. By alternating between different flow patterns, one can induce chaotic advection. Moreover, the stirrer can also operate with continuous, through flows. We demonstrated in both experiment and theory that it is possible to induce efficient stirring with this type of a MHD stirrer. Since there are no moving mechanical parts, similar (scaled down) stirrer designs are appropriate for various microfluidic applications. When reducing the device's size, one must keep in mind, however, that the Lorentz forces are volumetric in nature and decline rapidly in magnitude as the stirrer's volume decreases.

The MHD pump and stirrer described here are not completely problem-free. Some potential problems are bubble formation, electrode corrosion, and migration of analytes in the electric field. Most of these problems can, however, be reduced or eliminated altogether with appropriate selection of electrolytes, electrode materials and operating conditions. Bubble formation is not likely to be a problem at sufficiently low potential differences (smaller than the potential needed for the electrolysis of water). Electrode corrosion may be tolerated in disposable

devices or minimized with the use of passivated electrodes. RedOx solutions such as $FeCl_2$ / $FeCl_3$, potassium ferrocyanide trihydrate ($K_4[Fe(CN)_6]\times 3H_2O$) / potassium ferricyanide ($K_3[Fe(CN)_6]$), and hydroquinone in combination with inert electrodes provide relatively high current densities at low electrodes' potential differences without any electrode corrosion, bubble formation, and electrolyte depletion.

ACKNOWLEDGMENTS

Drs. Z. Chen, S-C Kweon, and J. Wang (University of Pennsylvania) assisted with the construction of the experiment. The work was supported, in part, by DARPA'S SIMBIOSYS PROGRAM (Dr. Anantha Krishnan, program director) through grant N66001-01-C-8056 to the University of Pennsylvania.

REFERENCES

[1] H. H. Woodson and J.R. Melcher, Electromechanical Dynamics, Vol. III, John Wiley, 1969

[2] P. A. Davidson, An Introduction to Magnetohydrodynamics, Cambridge Press, 2001

[3] J. Jang, S.S. Lee, Theoretical and Experimental Study of MHD (Magnetohydrodynamic) Micropump, Sensors and Actuators A, 80(2000), 84-89.

[4] A.V. Lemoff, A.P. Lee, An AC Magnetohydrodynamic Micropump, Sensors and Actuators B, 63 (2000), 178-185.

[5] H.H. Bau, A Case for Magneto-hydrodynamics (MHD), IMECE 2001, MEMS 23884 Symposium Proceedings, N.Y., Nov 2001

[6] J. Zhong, M. Yi, H.H. Bau, Magneto-hydrodynamic (MHD) Pump Fabricated with Ceramic Tapes, Sensors and Actuators A**,** 96 (2002), 59-66

[7] H.H. Bau, J. Zhong, and M. Yi, A Minute Magneto Hydro Dynamic (MHD) Mixer, Sensors and Actuators B, 79 (2001), 205-213.

[8] H.H. Bau, J. Zhu, S. Qian, Y. Xiang, A Magneto-Hydrodynamic Micro Fluidic Network, IMECE 2002-33559, Proceedings of IMECE'02, 2002 ASME International Mechanical Engineering Congress & Exposition, New Orleans, Louisiana, November 17-22, 2002

[9] H.H. Bau, J. Zhu, S. Qian, Y. Xiang, A Magneto-hydrodynamically Controlled Fluidic Network, Sensors and Actuators B, 88 (2003), 207-218

[10] J. West, B. Karamata, B. Lillis, J.P. Gleeson, J. Alderman, J.K. Collins, W. Lane, A. Mathewson, H. Berney, Application of Magnetohydrodynamic Actuation to Continuous Flow Chemistry, Lab on a Chip, 2 (2002), 224-230

[11] J. Gleeson and J. West, Magnetohydrodynamic Micromixing, Technical Proceedings of the Fifth International Conference on Modeling and Simulation of Microsystems, Puerto Rico, 318-321, 2002

[12] G. Taylor, Dispersion of Soluble Matter in Solvent Flowing Slowly through a Tube, Proceedings of the Royal Society of London Series A-Mathematical and Physical Sciences, 219 (1953),186-203.

[13] H. Aref, Stirring by Chaotic Advection, J. Fluid Mechanics, 143(1984), 1-21.

[14] M. Yi, S. Qian, H.H. Bau, A Magnetohydrodynamic Chaotic Stirrer, Journal of Fluid Mechanics, 468 (2002), 153-177

[15] S. Qian, J. Zhu , H.H. Bau, A Stirrer for Magnetohydrodynamically Controlled Minute Fluidic Networks, Physics of Fluids, 14 (2002), 3584-3592

[16] S. Qian, H.H. Bau, A Chaotic Electroosmotic Stirrer, Analytical Chemistry**,** 74 (2002), 3616-3625

[17] Y. Xiang, H.H. Bau, Complex Magnetohydrodynamic Low-Reynolds-Number Flows, Physical Review E, 68 (2003), 016312

[18] N. Kockmann, C. Föll, P. Woias, Flow Regimes and Mass Transfer Characteristics in Static Micro Mixers, SPIE 8982-38, Photonics West, Micromachining and Microfabrication, San Jose, January 27-29,2003.

[19] Y. K. Lee, J. Deval, P. Tabeling, and C.M. Ho, Chaotic Mixing in Electrokinetically and Pressure Driven Micro Flows, Proc. 14th IEEE workshop on Micro Electro Mechanical Systems (Interlaken, Switzerland) January 2001, 483-486

[20] M. H. Oddy, J. G. Santiago, and J. C. Mikkelsen, Electrokinetic Instability Micromixing, Analytical Chemistry, *73*(2002), 5822-5832

[21] E. Delamarche, H. Schmid, B. Michel, and H. Biebuyck, Stability of Molded Polydimethylsiloxane Microstructures, Advanced Materials, 9 (1997), 741-746

[22] J.A. Dean, Lange's Handbook of Chemistry, the 15th edition, New York: McGraw-Hill, 1999

LIST OF CAPTIONS

1. A schematic, top view of the stirrer's cavity. The cavity is equipped with numerous individual electrodes, (C_i^+) and (C_i^-), positioned along opposite walls. The length of each electrode is L_E, the gap between adjacent electrodes is c, and the electrodes are staggered with shift S.
2. The potential field (contours of constant potential) when the electrode pair C_0^- - C_1^+ is active with a potential difference $2.5V$. S=0, c/L_E=0.05, L/L_E =8.5, h/L_E=0.4, and H/L_E=0.4.
3. The simulated flow field in the vicinity of the active electrode pair C_0^- - C_1^+. The figure depicts the trajectories of passive tracer particles at the conduit's mid-height. The potential difference ΔV=2.5V, S=0, c/L_E=0.05, L/L_E =8.5, h/L_E=0.4, H/L_E=0.4, B=0.4T, and σ=2.56 $\Omega^{-1}m^{-1}$.
4. The spatial distribution of two initially separated fluids at the stirrer's midplane (z=H/2) and at various times: t=0(a), T/4 (b), T/2 (c), 3T/4 (d), T (e). Electrode pairs C_0^--C_1^+ and $C\text{-}_1^+$-C_0^- are activated alternately with a potential difference ΔV=2.5V and a period T=4s.
5. The spatial distribution of two initially separated fluids at cross-sections x= ($1.5L_E$+c) (I), x=0(II), and x=-($1.5L_E$+c) (III) and times t=0 (a), T/4 (b), T/2 (c), 3T/4 (d), and T(e). Electrode pairs C_0^--C_1^+ and $C\text{-}_1^+$-C_0^- are activated alternately with a potential difference ΔV=2.5V and a period T=4s.
6. The mixing quality (α) as a function of time at cross-sections x=$1.5L_E$+c (solid line), x=0 (dash-dot line), and x=-($1.5L_E$+c) (dashed line). Electrode pairs C_0^--C_1^+ and $C\text{-}_1^+$-C_0^- are alternately active with a potential difference ΔV=2.5V and a period T=4s.

7. The flow field and streak lines in the midplane (z=H/2) when electrode pair TO-BE is active with a potential difference ΔV=2.5V. The fluid flows continuously through the straight conduit with average axial velocity U=5mm/s. B=0.4T and σ=2.56 $\Omega^{-1}m^{-1}$.
8. The spatial distribution of two initially separated fluids at the midplane (z=H/2) at times t=0 (a), T/2(b), T(c), 3T/2(d), and 2T (e). The fluids flow continuously through the straight conduit with average axial velocity U=5mm/s. The electrode pairs TO-BE and BO-TE are alternately active with an imposed potential difference ΔV=2.5V and a period T=4s. B=0.4T, D=10^{-11} m^2/s and σ=2.56 $\Omega^{-1}m^{-1}$.
9. The spatial distribution of two initially separated fluids at cross-sections x=40mm (I) and x=70mm (II) and at times t=0 (a), t=T/2(b), t=T(c), t=3T/2 (d), and t=2T (e). The fluids flow continuously through the straight conduit with an average axial velocity U=5mm/s. The electrode pairs TO-BE and BO-TE are alternately active with an imposed potential difference ΔV=2.5V and a period T=4s. B=0.4T, D=10^{-11} m^2/s and σ=2.56 $\Omega^{-1}m^{-1}$.
10. The mixing quality α in the flow-through reactor as a function of time at cross-sections x=10mm (solid line and symbols ■), x=40mm (dashed line and symbols ●), and x=70mm (dash-dot line and symbols ▲). The fluids flow continuously through the straight conduit with an average axial velocity U=5mm/s. The electrode pairs TO-BE and BO-TE are alternately active with an imposed potential difference ΔV=2.5V and a period T=4s. B=0.4T, D=10^{-11} m^2/s, and σ=2.56 $\Omega^{-1}m^{-1}$.
11. The mixing quality α in the flow-through reactor as a function of *K* at x=40mm, t=4T, and T=4s.
12. A schematic description of the MHD stirrer (an exploded view).
13. The potential difference ΔV_{-1} between the inactive electrode C_{-1}^{+} and the ground electrode C_1^{+} as a function of the imposed potential difference ΔV_0 between the active

electrodes C_0^- - C_1^+. The solid line and the symbols (•) represent, respectively, the theoretical predictions and the measured values.

14. Flow visualization of the spread of a dye blob inserted in the stirrer at times t=0, T/2, T, 3T/2, 2T, 5/2T and 3T. The electrode pairs C_0^--C_1^+ and C_{-1}^+-C_0^+ are alternately active with a potential difference ΔV=2.5V and a period T=4s.
15. Images of the blending process when initially well-separated red and green dye blobs are introduced into the stirrer. The various images correspond to times t=0, T, 2T, 3, 4T, 5T, 6T, and 7T. The electrode pairs C_0^--C_1^+ and C_{-1}^+-C_0^+ are alternately active with a potential difference ΔV=2.5V and a period T=4s.
16. The spread of the dye in the flow-through stirrer at times t=0 (a, inactive stirrer), t=T/2 (b), t=T (c) and t=3T/2 (d). A potential difference of ΔV=2.0V is imposed between the active electrodes. Different pairs of electrodes are alternately engaged with a period T=4s. The average fluid velocity is 5mm/s, and the net flow rate is 2ml/s.

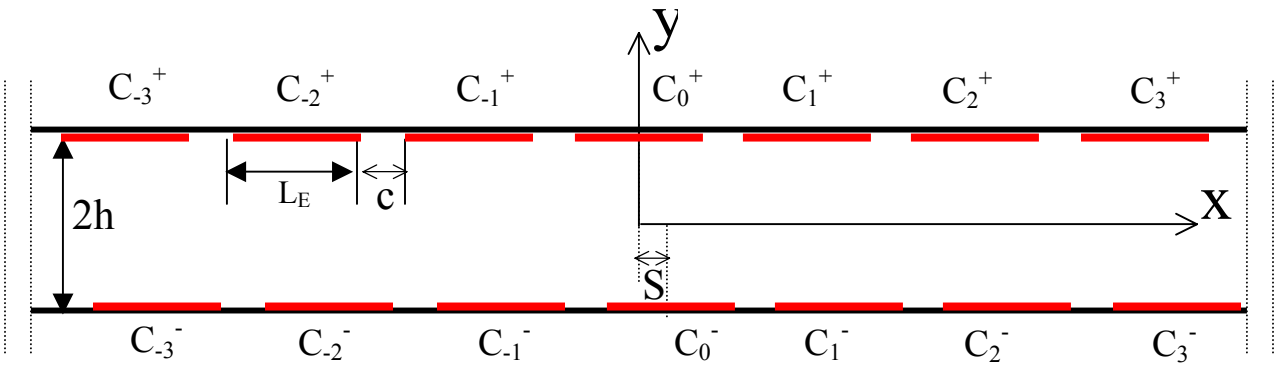

Fig.1: A schematic, top view of the stirrer's cavity. The cavity is equipped with numerous individual electrodes, (C_i^+) and (C_i^-), positioned along opposite walls. The length of each electrode is L_E, the gap between adjacent electrodes is c, and the electrodes are staggered with shift S.

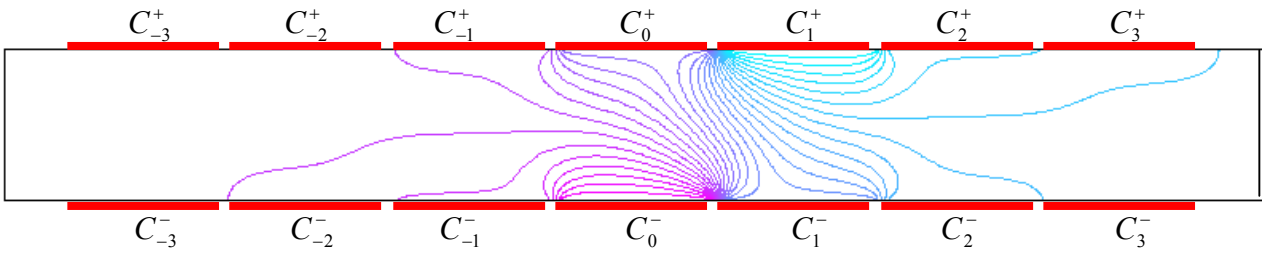

Fig.2: The potential field (contours of constant potential) when the electrode pair C_0^- - C_1^+ is active with a potential difference *2.5V*. S=0, c/L_E=0.05, L/L_E =8.5, h/L_E=0.4, and H/L_E=0.4.

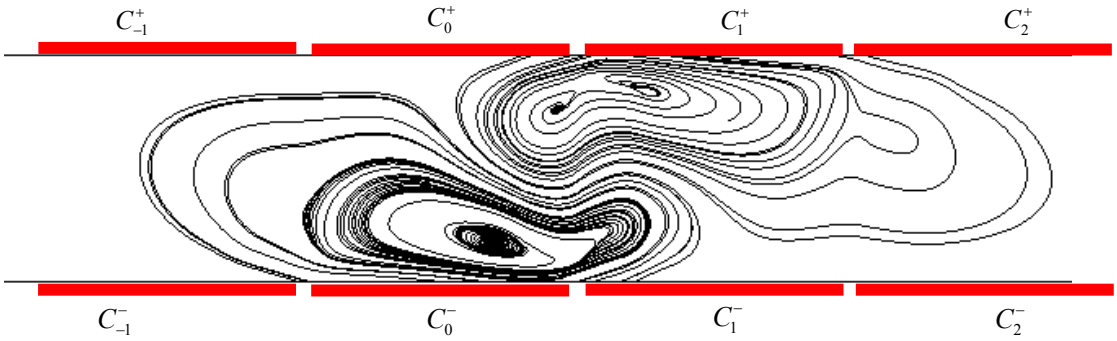

Fig.3: The simulated flow field in the vicinity of the active electrode pair C_0^- - C_1^+. The figure depicts the trajectories of passive tracer particles at the conduit's mid-height. The potential difference ΔV=2.5V, S=0, c/L_E=0.05, L/L_E =8.5, h/L_E=0.4, H/L_E=0.4, B=0.4T, and σ=2.56 $\Omega^{-1}m^{-1}$.

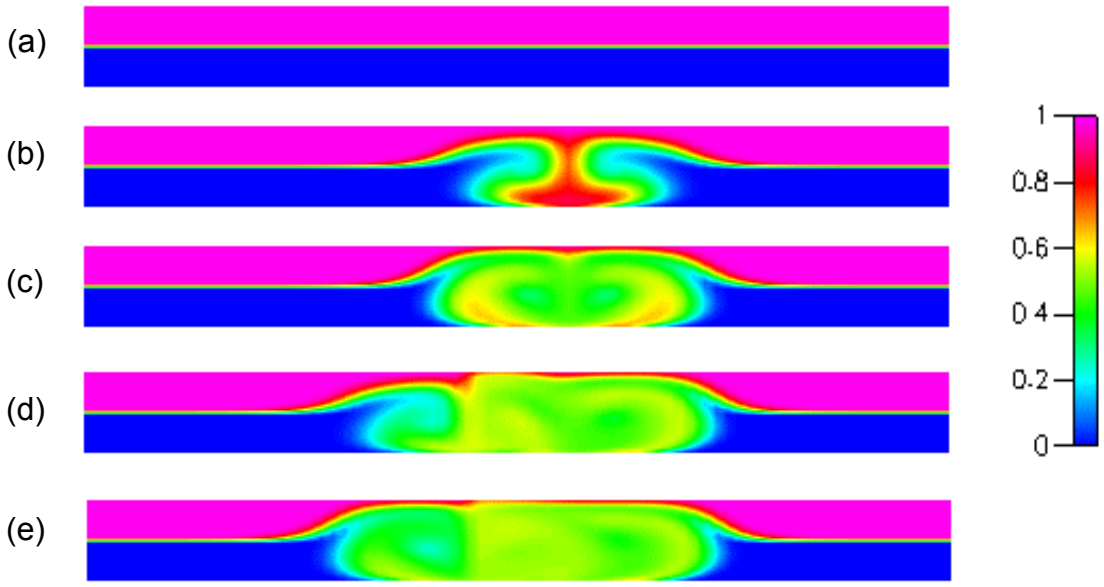

Fig. 4: The spatial distribution of two initially separated fluids at the stirrer's midplane (z=H/2) and at various times: t=0(a), T/4 (b), T/2 (c), 3T/4 (d), T (e). Electrode pairs C_0^--C_1^+ and C_{-1}^+-C_0^- are activated alternately with a potential difference ΔV=2.5V and a period T=4s.

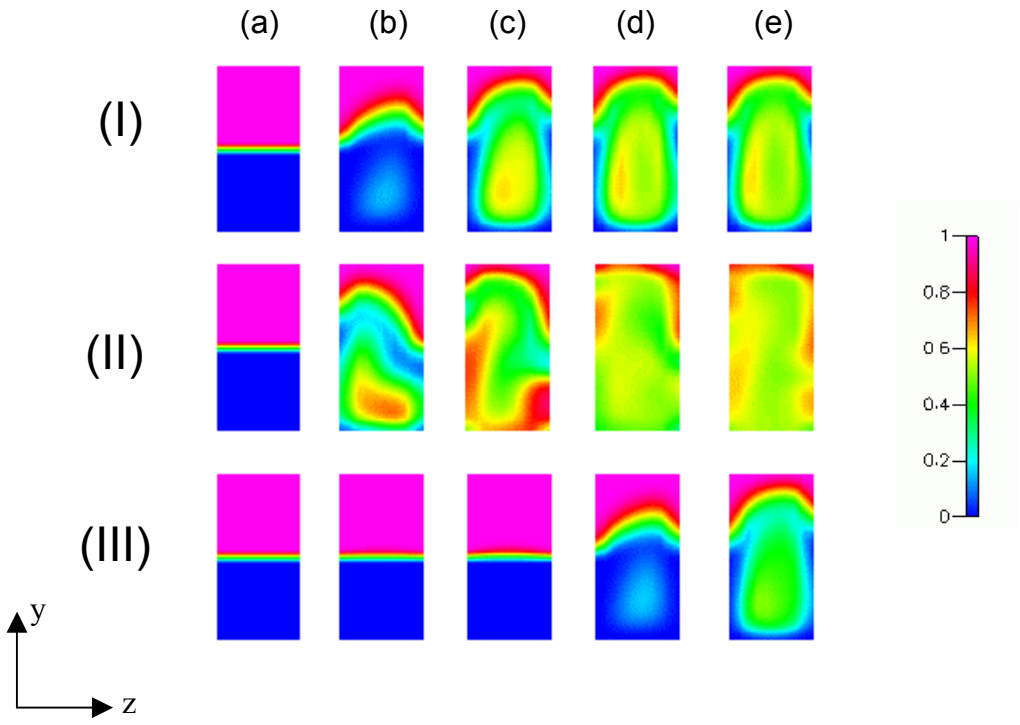

Fig.5: The spatial distribution of two initially separated fluids at cross-sections x= ($1.5L_E$+c) (I), x=0(II), and x=-($1.5L_E$+c) (III) and times t=0 (a), T/4 (b), T/2 (c), 3T/4 (d), and T(e). Electrode pairs C_0^--C_1^+ and C_{-1}^+-C_0^- are activated alternately with a potential difference ΔV=2.5V and a period T=4s.

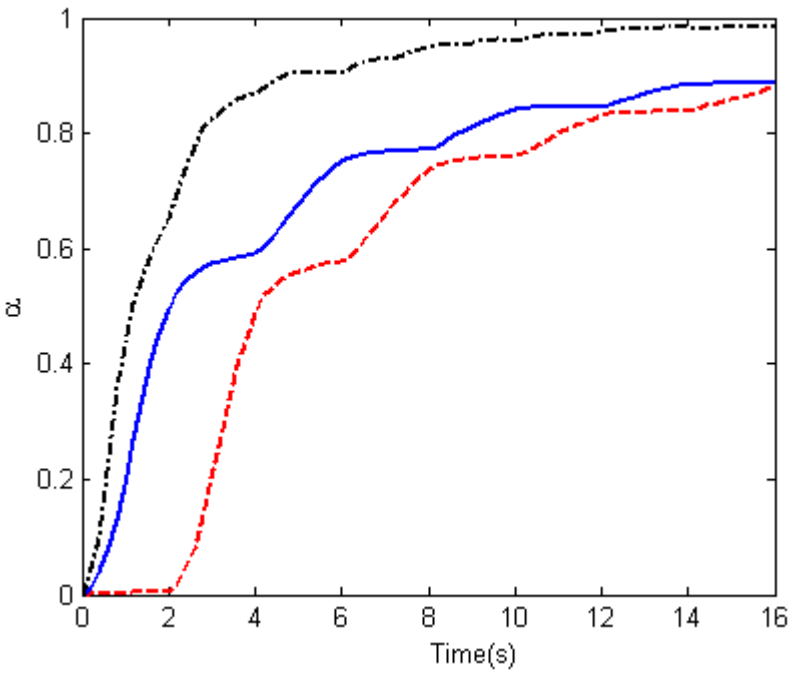

Fig.6: The mixing quality (α) as a function of time at cross-sections $x=1.5L_E+c$ (solid line), $x=0$ (dash-dot line), and $x=-(1.5L_E+c)$ (dashed line). Electrode pairs C_0^--C_1^+ and C_{-1}^+-C_0^- are alternately active with a potential difference $\Delta V=2.5V$ and a period $T=4s$.

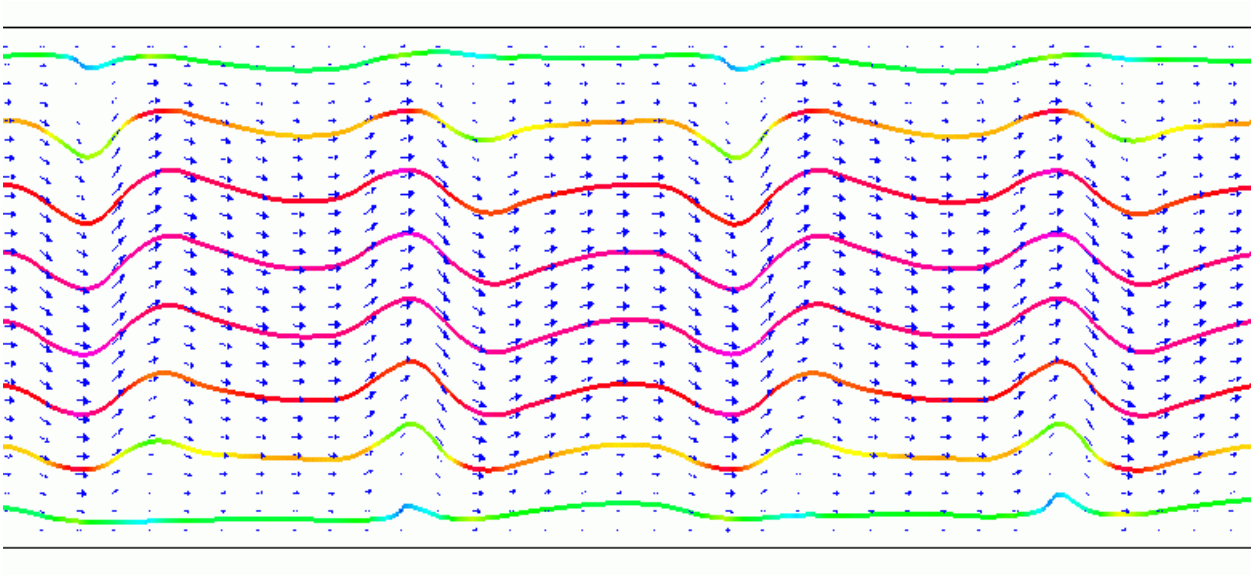

Fig. 7: The flow field and streak lines in the midplane (z=H/2) when electrode pair TO-BE is active with a potential difference $\Delta V=2.5V$. The fluid flows continuously through the straight conduit with average axial velocity U=5mm/s. B=0.4T and $\sigma=2.56\ \Omega^{-1}m^{-1}$.

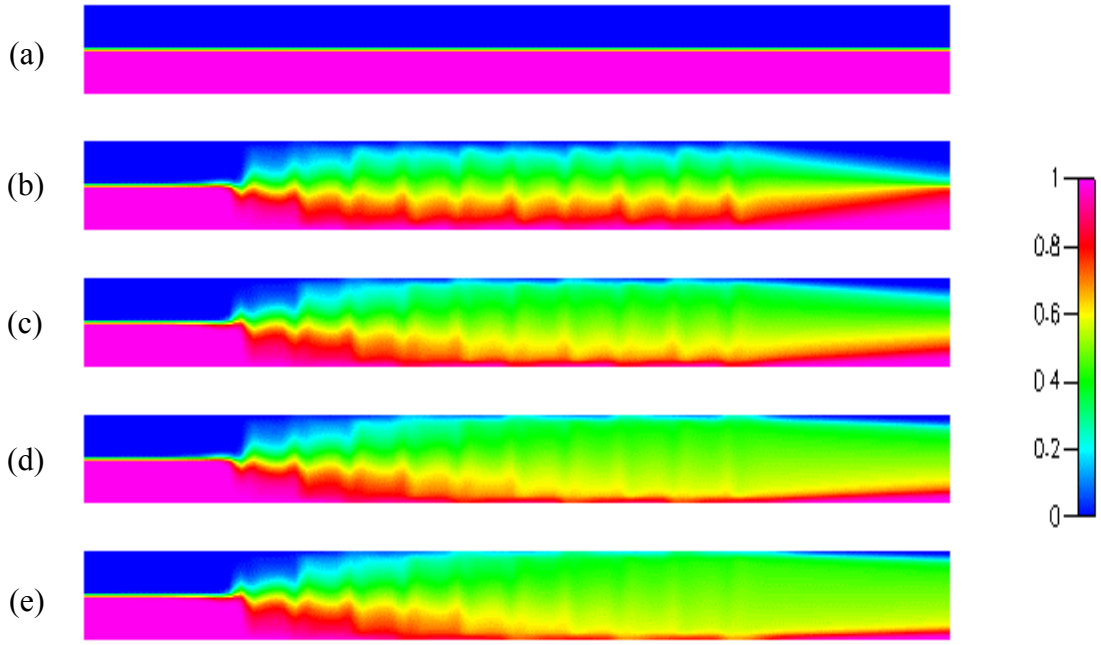

Fig.8: The spatial distribution of two initially separated fluids at the midplane (z=H/2) at times t=0 (a), T/2(b), T(c), 3T/2(d), and 2T (e). The fluids flow continuously through the straight conduit with average axial velocity U=5mm/s. The electrode pairs TO-BE and BO-TE are alternately active with an imposed potential difference ΔV=2.5V and a period T=4s. B=0.4T, D=10^{-11} m^2/s and σ=2.56 $\Omega^{-1}m^{-1}$.

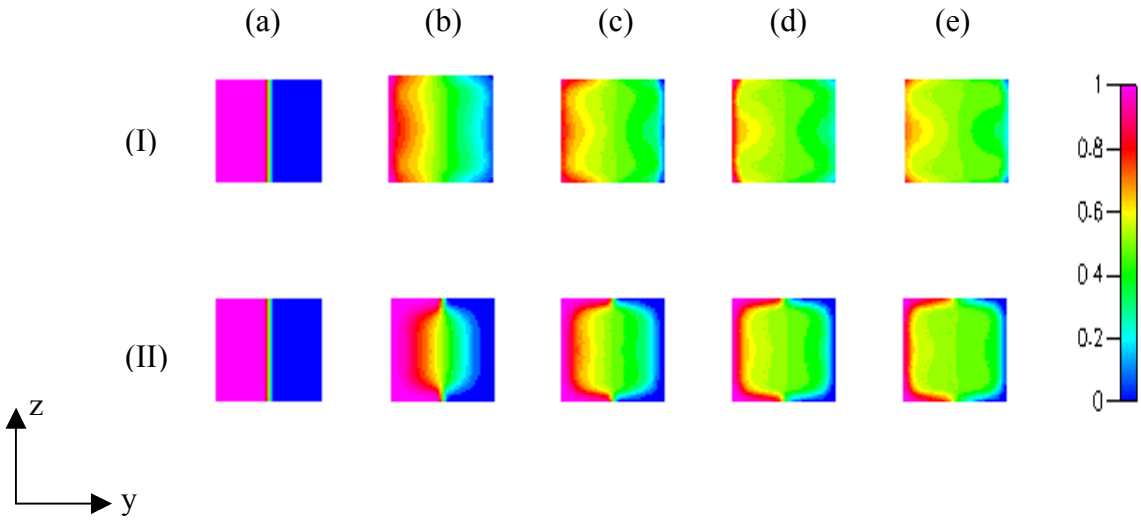

Fig.9: The spatial distribution of two initially separated fluids at cross-sections x=40mm (I) and x=70mm (II) and at times t=0 (a), t=T/2(b), t=T(c), t=3T/2 (d), and t=2T (e). The fluids flow continuously through the straight conduit with an average axial velocity U=5mm/s. The electrode pairs TO-BE and BO-TE are alternately active with an imposed potential difference ΔV=2.5V and a period T=4s. B=0.4T, D=10^{-11} m^2/s and σ=2.56 $\Omega^{-1}m^{-1}$.

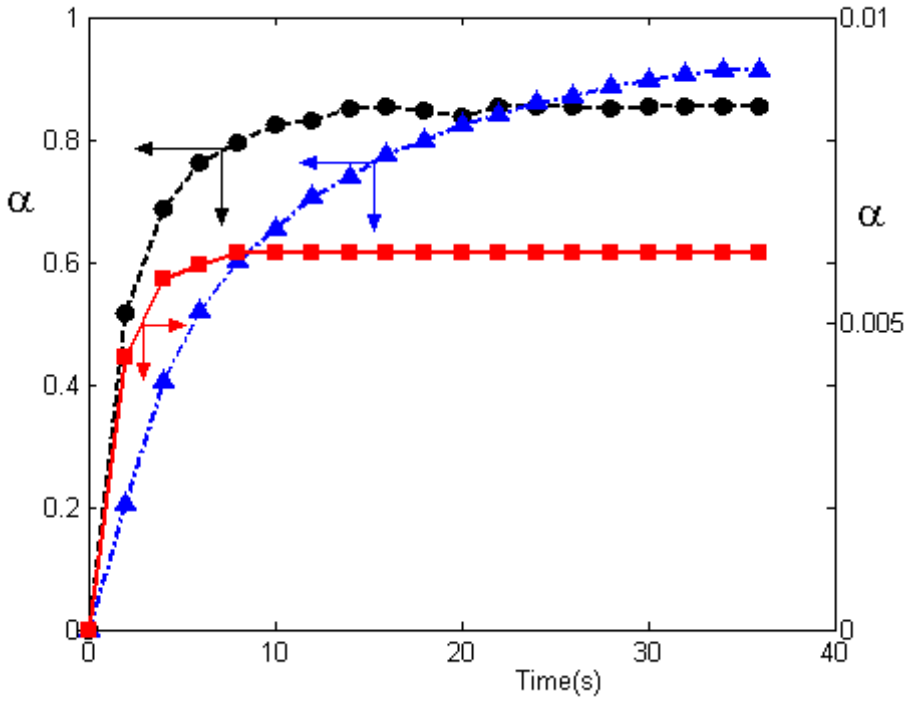

Fig.10: The mixing quality α in the flow-through reactor as a function of time at cross-sections x=10mm (solid line and symbols ■), x=40mm (dashed line and symbols ●), and x=70mm (dash-dot line and symbols ▲). The fluids flow continuously through the straight conduit with an average axial velocity U=5mm/s. The electrode pairs TO-BE and BO-TE are alternately active with an imposed potential difference ΔV=2.5V and a period T=4s. B=0.4T, $D=10^{-11}$ m^2/s, and $\sigma=2.56$ $\Omega^{-1}m^{-1}$.

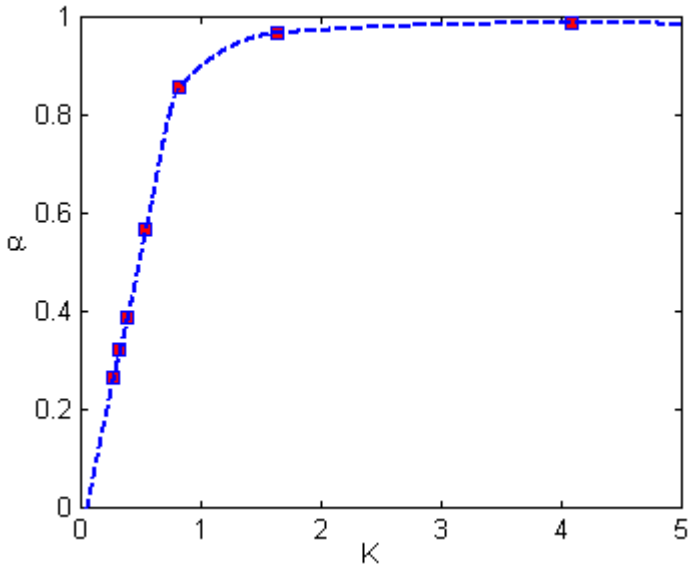

Fig.11: The mixing quality α in the flow-through reactor as a function of *K* at x=40mm, t=4T, and T=4s.

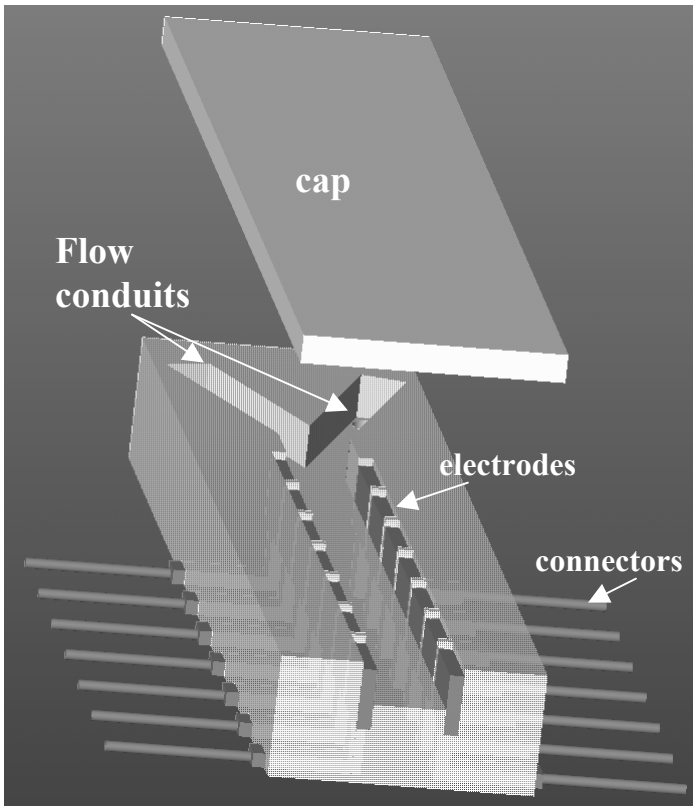

Fig.12: A schematic description of the MHD stirrer.

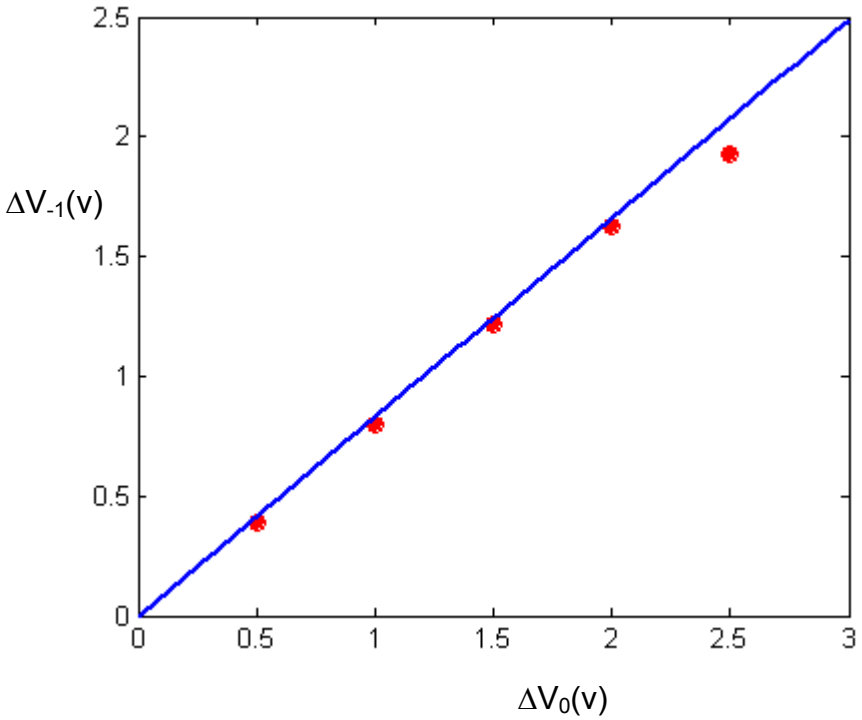

Fig.13: The potential difference ΔV_{-1} between the inactive electrode C_{-1}^{+} and the ground electrode C_1^{+} as a function of the imposed potential difference ΔV_0 between the active electrodes C_0^{-} - C_1^{+}. The solid line and the symbols (•) represent, respectively, the theoretical predictions and the measured values.

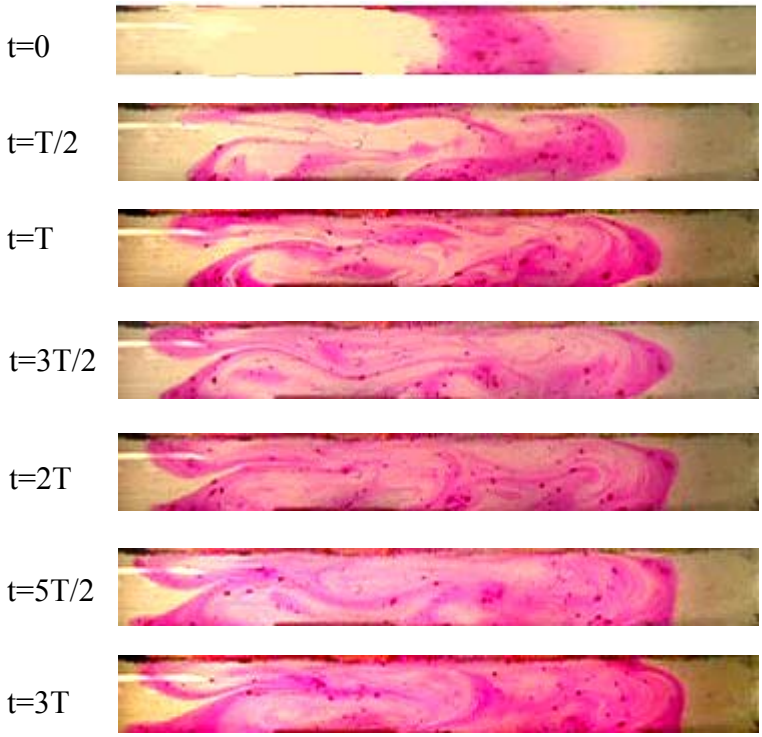

Fig.14**:** Flow visualization of the spread of a dye blob inserted in the stirrer at times t=0, T/2, T, 3T/2, 2T, 5/2T and 3T. The electrode pairs C_0^--C_1^+ and C_{-1}^+-C_0^+ are alternately active with a potential difference ΔV=2.5V and a period T=4s.

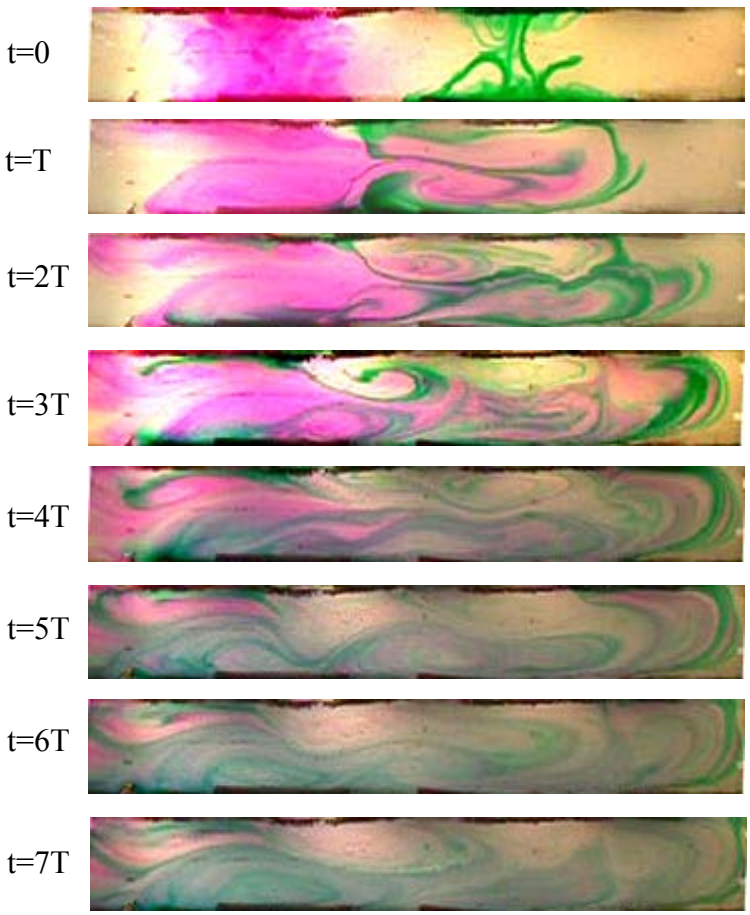

Fig. 15**:** Images of the blending process when initially well-separated red and green dye blobs are introduced into the stirrer. The various images correspond to times t=0, T, 2T, 3, 4T, 5T, 6T, and 7T. The electrode pairs C_0^--C_1^+ and C_{-1}^+-C_0^+ are alternately active with a potential difference ΔV=2.5V and a period T=4s.

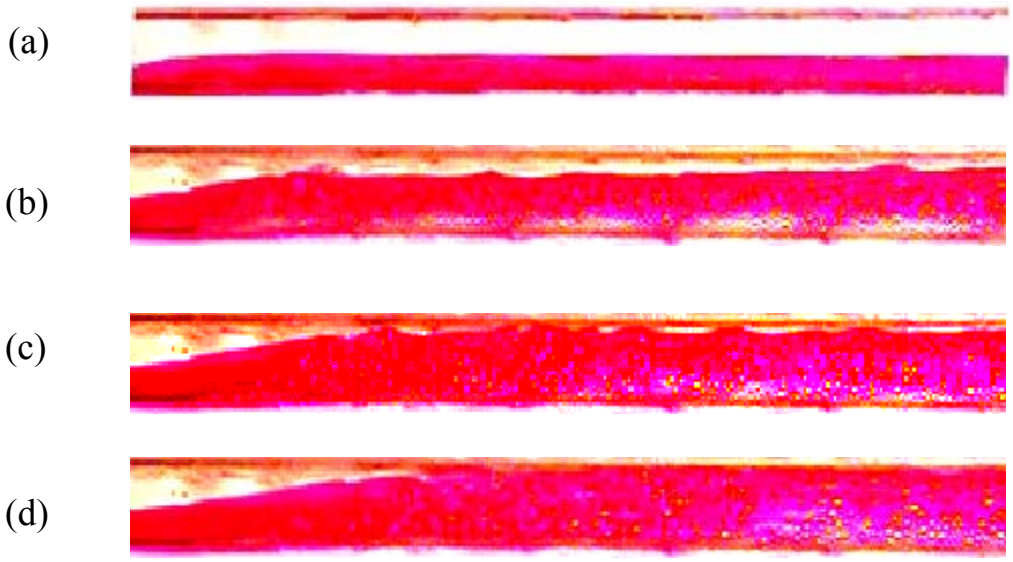

Fig.16: The spread of the dye in the flow-through stirrer at times t=0 (a, inactive stirrer), t=T/2 (b), t=T (c) and t=3T/2 (d). A potential difference of ΔV=2.0V is imposed between the active electrodes. Different pairs of electrodes are alternately engaged with a period T=4s. The average fluid velocity is 5mm/s, and the net flow rate is 2ml/s.